

Visual Autoregressive Modelling for Monocular Depth Estimation

Amir El-Ghoussani¹ ^a, André Kaup¹ ^b, Nassir Navab² ^c, Gustavo Carneiro³ ^d and Vasileios Belagiannis¹ ^e

¹*Friedrich-Alexander University Erlangen-Nuremberg, Germany*

²*Technical University of Munich, Germany*

³*University of Surrey, United Kingdom*

amir.el-ghoussani@fau.de

Keywords: Monocular Depth Estimation, Visual Autoregressive Modelling

Abstract: We propose a monocular depth estimation method based on visual autoregressive (VAR) priors, offering an alternative to diffusion-based approaches. Our method adapts a large-scale text-to-image VAR model and introduces a scale-wise conditional upsampling mechanism with classifier-free guidance. Our approach performs inference in ten fixed autoregressive stages, requiring only 74K synthetic samples for fine-tuning, and achieves competitive results. We report state-of-the-art performance in indoor benchmarks under constrained training conditions, and strong performance when applied to outdoor datasets. This work establishes autoregressive priors as a complementary family of geometry-aware generative models for depth estimation, highlighting advantages in data scalability, and adaptability to 3D vision tasks. Code available at "<https://github.com/AmirMaEl/VAR-Depth>".

1 Introduction

Monocular depth estimation, a fundamental task in computer vision, involves predicting the depth of a scene from a single 2D image. At the same time, it is an inherently ill-posed problem. The process of capturing a 3D scene on a 2D sensor inevitably results in the loss of explicit depth information. Inferring 3D structure from 2D projections presents several challenges. First, scale ambiguity, where objects of varying sizes at different distances can produce identical 2D projections. Second, perspective ambiguity, as similar shapes at different orientations can result in indistinguishable 2D representations. Finally, occlusions can lead to incomplete depth information. Fortunately, deep neural networks partially address these challenges.

Earlier approaches to monocular depth estimation relied on supervised learning techniques (Eigen et al., 2014; Liu et al., 2016; Laina et al., 2016), which directly regressed depth from RGB inputs

through convolutional neural networks. A significant paradigm shift occurred with the introduction of self-supervised methods (Yin et al., 2018; Godard et al., 2017; Zhou et al., 2017) that reduced the need for ground truth depth annotations by exploiting geometric constraints. These methods not only minimized annotation requirements but also allowed the use of vast, readily available datasets, significantly expanding the scope of training data in the field. More recently, advancements have been driven by the availability of large-scale training datasets (Ranftl et al., 2020, 2021). This shift towards extensive data collection, combined with increasingly sophisticated neural network architectures, has enabled models to learn robust visual priors for depth prediction, at the cost of large training datasets. Despite their impressive results, these approaches contain significant computational overhead and extended training periods.

The latest advancements incorporate generative models (Zhang et al., 2024) and adapt large diffusion models (Ke et al., 2024; Gui et al., 2025) for depth estimation, treating it as a conditional image generation task. However, these methods inherently rely on computationally expensive diffusion priors learned from massive datasets, often involving billions of image-text pairs (Fu et al., 2025; Gui et al., 2025).

In this work, we explore visual autoregressive

^a <https://orcid.org/0009-0009-5645-6684>

^b <https://orcid.org/0000-0002-0929-5074>

^c <https://orcid.org/0000-0002-6032-5611>

^d <https://orcid.org/0000-0002-5571-6220>

^e <https://orcid.org/0000-0003-0960-8453>

(VAR) modeling as an alternative to diffusion-based depth estimation. Although still slightly slower than a single feedforward pass, VAR models generate images hierarchically in a few-step process, and can be pretrained on fewer samples while retaining strong generative priors. Building on Switti (Voronov et al., 2024), a large text-to-image VAR model trained on approximately 100 million image–text pairs, we adapt visual autoregression to affine-invariant depth estimation with three key design choices. First, we introduce a scale-wise conditional upsampling mechanism that propagates geometric cues across resolutions. Second, we design a guidance rule that balances contributions from the autoregressive prior and the conditional upsample. Third, we propose a re-encoding strategy that enables intermediate predictions without requiring multiple upsamples per scale. Fine-tuning relies solely on 74K synthetic images (Hypersim and vKITTI), keeping data requirements modest.

Our experiments demonstrate that VAR priors are a viable alternative to diffusion-based approaches. We report competitive indoor performance on NYUv2 and ScanNet, and reasonable outdoor results on KITTI, ETH3D, and DIODE. Beyond accuracy, our analysis compares sampling speed and the trade-offs associated with model size and training cost.

2 Related work

2.1 Monocular Depth Estimation

With the rapid development of deep neural networks, monocular depth estimation with the help of deep learning has been widely studied. Various supervised learning approaches have been proposed in recent years. The seminal paper of Eigen et al. (Eigen et al., 2014) introduced a CNN-based approach to directly regress the depth. Liu et al. (Liu et al., 2016) propose utilising a fully-connected CRF as a post-processing step to refine monocular depth predictions. Other methods have extended the CNN-based network by changing the regression loss to a classification loss (Wang et al., 2018; Yin et al., 2018; Bhat et al., 2021; Laina et al., 2016) or change the architecture of the depth estimation network entirely (Liu et al., 2023; Rudolph et al., 2022; Richter et al., 2016). To address data scarcity and domain shift when training across different datasets, several works have explored domain adaptation techniques for monocular depth estimation, particularly leveraging synthetic-to-real transfer (Kundu et al., 2018; El-Ghoussani et al., 2025).

More recent advancement of depth estimation

models has been marked by increasing model and dataset scales. MiDaS (Ranftl et al., 2020) established early benchmarks through multi-dataset training, followed by DPT (Ranftl et al., 2021) and Omnidata (Eftekhar et al., 2021) leveraging ViT architectures (Ranftl et al., 2021). Recent works like DepthAnything (Yang et al., 2024) and Metric3D (Hu et al., 2024) further push boundaries by utilizing DINov2 backbones (Oquab et al., 2023) and substantially larger datasets.

To reduce dependence on large training datasets, research has also explored the use of generative models, particularly diffusion models, for monocular depth estimation. DDP (Saxena et al., 2024) introduces an encoder-decoder architecture that achieves state-of-the-art results on the KITTI benchmark (Geiger et al., 2013). DepthGen (Saxena et al., 2023) expands multi-task diffusion frameworks to include metric depth prediction, while DDVM (Saxena et al., 2023) utilizes both synthetic and real data during pre-training to improve depth estimation performance.

A significant advancement in this field is Marigold (Ke et al., 2024), which adapts Stable Diffusion (Esser et al., 2021) for MDE, using only synthetic data during this finetuning process. However, it relies on a diffusion prior, in particular Marigold uses SD 2.0 (Rombach et al., 2022) which is trained on LAION-5B (Schuhmann et al., 2022). Instead, our method employs a generative VAR prior, i.e. Switti (Voronov et al., 2024), which was effectively trained using a significantly more constrained dataset of only 100 million samples.

To the best of our knowledge this work presents the first approach that is derived from a pre-trained text-to-image VAR model specifically designed for affine-invariant depth estimation.

2.2 Autoregressive Modelling

Autoregressive models have transformed the image generation task. Starting with PixelCNN (Van den Oord et al., 2016), which predicted RGB values sequentially in raster scan order, the field evolved when (Van Den Oord et al., 2017) showed images could be compressed into discrete tokens. VQGAN (Esser et al., 2021) later enhanced this approach by integrating adversarial and perceptual losses. Newer research focused on hierarchical and multi-scale approaches. VQVAE-2 (Razavi et al., 2019) used multi-level latent variables to capture both global and local features, while RQTransformer (Lee et al., 2022) enhanced this with residual quantization. Parti (Yu et al., 2022) scaled the ViT-VQGAN architecture to 20 billion parameters, achieving state-of-the-art text-

to-image generation. MaskGIT (Chang et al., 2022) introduced masked prediction in VQ latent space, which was later adapted for video in MagViT models (Yu et al., 2023, 2022). MUSE (Chang et al., 2023) integrated the T5 language model (Raffel et al., 2020), strengthening text-image connections for better prompt responsiveness. More recent advances in autoregressive image generation have integrated advanced language modelling architectures. LLamaGen (Sun et al., 2024) adapts the Llama foundation model (Touvron et al., 2023) for image synthesis, while AiM (Li et al., 2024) incorporates Mamba’s selective state space modeling (Gu and Dao, 2023). Lumina-mGPT (Liu et al., 2024) extends this trend with a family of multimodal autoregressive models optimized for photorealistic image generation.

Visual Autoregressive Modelling (VAR) (Tian et al., 2024) has recently achieved promising results in image generation by predicting entire resolution levels at once through next-scale prediction, thereby reducing the computational overhead while maintaining the high quality of the output. Several works have extended VAR to text-to-image generation: Switti (Voronov et al., 2024) implements text-image alignment via cross-attention modules. Similarly, Infinity (Han et al., 2025) uses cross-attention for alignment while introducing an infinite-vocabulary optimizer and bitwise self-correction mechanisms to accelerate training. Infinity is trained on a combined dataset of LAION (Schuhmann et al., 2021), COYO (Byeon et al., 2022), and OpenImages (Kuznetsova et al., 2020). Building on these advances, we extend VAR beyond image synthesis, introducing a visual autoregressive prior explicitly adapted for monocular depth estimation. This establishes a new family of geometry priors, complementary to diffusion.

To the best of our knowledge this work presents the first approach that is derived from a pre-trained text-to-image VAR model specifically designed for affine-invariant depth estimation.

3 Method

Given the input RGB image $\mathbf{x} \in \mathbb{R}^{H \times W \times 3}$, our goal is to predict the depth map $\mathbf{d} \in \mathbb{R}^{H \times W \times 1}$ through an autoregressive process that decomposes the distribution $p(\mathbf{d}|\mathbf{x})$ into a sequence of conditional predictions. Inspired by VAR (Tian et al., 2024), we propose a multi-scale autoregressive approach to accelerate sequential depth prediction. The central component of our method is the integration of a prior, where we leverage pre-trained large-scale text-to-image VAR model and combine it with a custom conditional upsampling

mechanism. This upsampling operates across the k hierarchical VAR generation scales, progressively refining tokens from scale $k \rightarrow k+1$.

Our method is built on a hierarchical encoding and decoding scheme, which enables multi-scale representation and efficient autoregressive modelling (Sec.3.1). To effectively utilize the prior, we adopt a fine-tuning strategy that adapts the pre-trained VAR model to the depth estimation task (Sec. 3.2). Additionally, we design a conditional upsampling procedure that works with the prior, ensuring high-quality depth refinement during the upsampling process (Sec.3.3). Finally, we detail the sampling process, in which we use a custom guidance strategy to combine both prior utilization and conditional upsampling (Sec.3.4).

3.1 Background: Visual Autoregressive Modelling

VAR modelling (Tian et al., 2024) establishes a hierarchical representation through a multi-scale VQ-GAN (Esser et al., 2021) encoder, which transforms input images into a sequence of discrete token maps at progressively increasing resolutions. A transformer is then trained to autoregressively predict each higher resolution token map, conditioned on all preceding lower resolution maps.

Encoding and Codebook Lookup. Formally, during encoding, the image is transformed into K token maps $R = (\mathbf{r}_1, \mathbf{r}_2, \dots, \mathbf{r}_K)$, where \mathbf{r}_1 is the start token with 1×1 image size and \mathbf{r}_K corresponds to the token map with original encoded image size, i.e., $h \times w = h_K \times w_K$. The likelihood of each scale k is factorized autoregressively across all scales k .

All token maps in R share a common codebook $\mathcal{Z} \in \mathbb{R}^{V \times C}$, encoded via the encoder \mathcal{E} and decoder \mathcal{D} . Here, V denotes the vocabulary size and C the number of channels. Initially, an input \mathbf{x} is converted to an embedding feature map $\mathbf{f} = \mathcal{E}(\mathbf{x})$ with $\mathbf{f} \in \mathbb{R}^{h \times w \times C}$, and subsequently interpolated to build $\mathbf{f}_k = \mathcal{E}_k(\mathbf{f}) \in \mathbb{R}^{h_k \times w_k \times C}$. \mathcal{E}_k is defined as encoding the input with the encoder $\mathcal{E}(\cdot)$ with a subsequent interpolation to the current scale k . The feature map \mathbf{f}_k is then mapped to a codebook entry $\mathbf{r}_k \in [V]^{h_k \times w_k}$ of the codebook \mathcal{Z} via the closest Euclidean distance:

$$\mathbf{r}_k = Q(\mathbf{f}_k) = \left(\arg \min_{\mathbf{v} \in \mathcal{Z}} \|\mathbf{v} - \mathbf{f}_k\|_2 \right), \quad (1)$$

where \mathbf{v} represents one of the C -dimensional vectors from codebook \mathcal{Z} , and $Q(\cdot)$ denotes the quantization operation. The resulting multi-scale discrete tokens

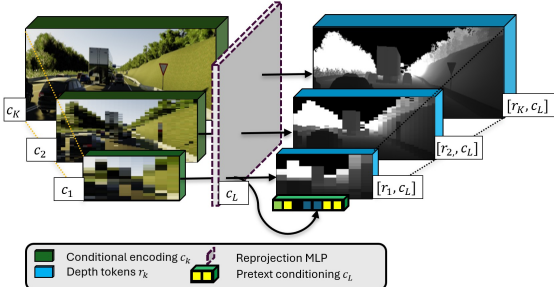


Figure 1: Overview of the proposed fine-tuning protocol. During model training the RGB image \mathbf{c}_k is reprojected using a MLP to align the dimension \mathbf{c}_k with the text dimension \mathbf{c}_L . The modified input each scale k to the VAR transformer then consists of both the ground truth depth token \mathbf{r}_k and the conditional encoding \mathbf{c}_L .

$\mathbf{r}_1, \mathbf{r}_2, \dots, \mathbf{r}_k$ with $\mathbf{r}_k \in V^{h_k \times w_k}$ forms the foundation for autoregressive modelling.

$$\hat{\mathbf{f}} = \sum_{k=1}^K \theta(\mathbf{f}_k) = \sum_{k=1}^K \theta(Q^{-1}(\mathbf{r}_k)). \quad (2)$$

Decoding. The decoder \mathcal{D} processes the combined feature representation $\hat{\mathbf{f}}$ to produce the final decoded output, such that $\mathcal{D}(\hat{\mathbf{f}}) = \hat{\mathbf{x}}$. To address information loss during upsampling, a network $\{\theta\}_{k=1}^K$ consisting of K convolution layers is used.

We keep this standard formulation unchanged and focus on extending it with depth-specific conditioning and sampling strategies.

3.2 Prior Model

We adopt the pre-trained text-to-image model Switti (Voronov et al., 2024), which was trained in a two-stage process. Initial pretraining utilized 100 million high-quality, re-captioned image-text pairs filtered from a larger web dataset, progressing from 256x256 to 512x512 resolution. This was followed by supervised fine-tuning on approximately 40,000 manually selected, highly aesthetic and detailed text-image pairs at 1024x1024 resolution.

Our contribution in this stage is to extend Switti into a depth-conditioned VAR model by introducing a conditional fine-tuning phase, described in the following section.

Conditional fine-tuning. To adapt the pretrained VAR prior to depth estimation, we first replace the standard text-to-image encoder with a projection MLP $f(\cdot)$ that maps conditional encodings \mathbf{c} into the text encoding space L :

$$\mathbf{c}_L = f(\mathbf{c}_k). \quad (3)$$

The dimensionality of \mathbf{c}_L is independent of the scale \mathbf{c}_k , and \mathbf{c}_L is used as the conditioning signal for the transformer.

We then train the model using the teacher forcing paradigm established by (Tian et al., 2024), following a progressive resolution strategy—starting at 256×256 , advancing to 512×512 , and finally reaching 1024×1024 . For conditional fine-tuning both the depth tokens \mathbf{r}_k and the conditional RGB encodings \mathbf{c}_L are jointly processed during training. Training optimizes next-token prediction, where the model is trained to predict target token distributions based on previously observed tokens and conditioning features. The loss function is defined as:

$$\mathcal{L}_{\text{TF}} = -\mathbb{E}_{\mathbf{r}, \mathbf{c} \sim p_{\text{data}}} \left[\sum_{k=1}^K \log p_{\theta}(\mathbf{r}_k | \mathbf{r}_{<k}, \mathbf{c}_L) \right], \quad (4)$$

where \mathbf{r}_k represents tokens at the current scale k , $\mathbf{r}_{<k}$ denotes all tokens from previous scales, \mathbf{c}_L are the conditional encodings, p_{data} is the empirical data distribution, and p_{θ} is the model’s predicted probability distribution.

3.3 Conditional upsampling

Conventional transformer conditioning appends conditional tokens to the input sequence. This ensures that predictions are based on both input and conditional tokens at each step. However, for complex geometric information (rather than simple textual prompts or classes), we have empirically observed that this signal does not propagate effectively through the Switti transformer across scales. This issue arises from the learned upsampling layer $\theta(\cdot)$ of Eq. 2, which compresses or loses critical geometric context as information passes through generation scales k .

To overcome this limitation, we propose to replace the standard learned upsampling layer $\theta(\mathbf{f}_k)$, as shown in Eq. 2, with a conditional upsampling layer $U(\mathbf{f}_k, \mathbf{c}_k)$ that operates after the geometric upsampling operation. This conditional layer leverages an image-to-image model $U(\cdot)$ to predict the next token during the upscaling process:

$$\hat{\mathbf{f}}_{k+1} = U(\hat{\mathbf{f}}_k, \mathbf{c}_k). \quad (5)$$

Here, $\hat{\mathbf{f}}_{k+1}$ represents the upsampled and predicted version of the previous token encoding $\hat{\mathbf{f}}_k$, upsampled to dimensions h_{k+1} and w_{k+1} using the upscaling network $U(\cdot)$. Notably, the network $U(\cdot)$ operates directly on continuous token encodings \mathbf{f} and \mathbf{c}_k , rather than discrete tokenized representations \mathbf{r}_k and \mathbf{q}_k .

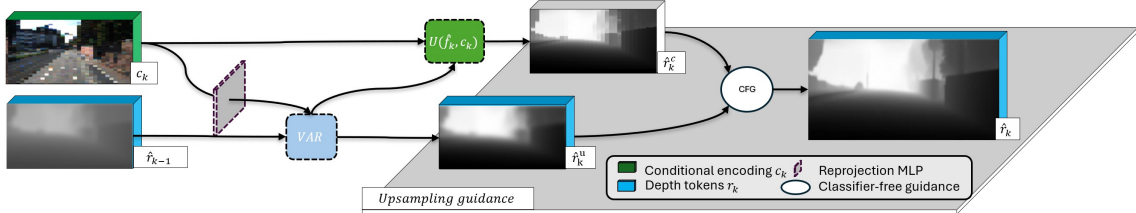


Figure 2: Overview of proposed sampling procedure. During sampling the prediction from the previous scale $\hat{\mathbf{r}}_{k-1}$ and the conditional reprojection encodings \mathbf{c}_L are processed by the VAR transformer. After this processing step the VAR prediction $\hat{\mathbf{r}}_k^u = \hat{\mathbf{r}}_k$ is fed into the conditional upsampling network $U(\cdot)$, along with the condition encoding \mathbf{c}_L to predict the output $\hat{\mathbf{r}}_k^c$. Finally both components are combined using classifier-free guidance to form the upsampled depth prediction $\hat{\mathbf{r}}_k$.

Table 1: Results obtained for the evaluation on all datasets, NYU (Nathan Silberman and Fergus, 2012), KITTI (Geiger et al., 2013), ETH3D (Schöps et al., 2019), ScanNet (Dai et al., 2017) and DIODE (Vasiljevic et al., 2019). Baselines are sourced from Metric3D (Hu et al., 2024). Bold numbers represent the best performing method. We only compare to methods that use $< 3M$ datasamples for finetuning and use a prior trained with $\leq 100M$ samples. Best results are **bold**, second best results are underlined.

Method	Prior	training samples	NYU		KITTI		ETH3D		ScanNet		DIODE	
			AbsRel \downarrow	$\delta_1 \uparrow$								
DepthAnything v2	DINOv2 - 142M	63M	4.4	97.9	7.5	94.8	13.2	86.2	—	—	6.5	95.4
	Metric3D	16M	5.8	96.1	10.1	90.9	6.6	95.8	6.6	95.0	31.7	77.2
Marigold	SD - 2.3B	74K	5.8	96.1	10.1	90.9	6.6	95.8	6.6	95.0	31.7	77.2
Marigold v1.1	SD - 2.3B	74K	5.5	96.4	10.5	90.2	6.9	95.7	5.8	96.3	29.8	78.2
DepthFM	SD - 2.3B	63K	6.5	95.6	8.3	93.4	—	—	—	—	22.5	80.0
Marigold E2E	SD - 2.3B	74K	5.2	96.6	9.6	91.9	6.2	95.9	5.8	96.2	30.2	77.9
DiverseDepth	ImageNet - 1M	320K	11.7	87.5	19.0	70.4	22.8	69.4	10.9	88.2	37.6	63.1
	MiDaS	2M	11.1	88.5	23.6	63.0	18.4	75.2	12.1	84.6	33.2	71.5
	LeReS	ImageNet - 1M	354K	9.0	91.6	14.9	78.4	17.1	77.7	9.1	91.7	27.1
	HDN	ImageNet - 14M	300K	6.9	94.8	11.5	86.7	12.1	83.3	8.0	93.9	24.6
	DPT	ImageNet - 14M	1.4M	9.8	90.3	10.0	90.3	7.8	94.6	<u>8.2</u>	<u>93.4</u>	18.2
Ours - optimized w_k	Switti - 100M	74K	6.4	94.8	<u>10.4</u>	<u>90.1</u>	<u>8.1</u>	<u>92.2</u>	7.9	<u>93.4</u>	<u>22.3</u>	75.4

We initialize $U(\cdot)$ with a U-Net (Ronneberger et al., 2015) using a timestep-aware approach, where the time step corresponds to step k . At each scale k , the model is trained to predict the final depth image \mathbf{f} given the corresponding image encodings \mathbf{c}_k . During training, we minimize the \mathcal{L}_2 -loss according to:

$$\mathcal{L} = \|U_k(\mathbf{f}_{k-1}, \mathbf{c}_{k-1}) - \mathbf{f}\|_2, \quad (6)$$

where U_k represents the image-to-image model at scale k . \mathbf{f}_{k-1} is the ground truth token and \mathbf{c}_{k-1} the RGB image condition encoding from the previous scale $k-1$.

This formulation enables the network to upsample the previous prediction $\hat{\mathbf{f}}_{k-1}$ to dimensions h_k, w_k , while effectively only requiring prediction of the residual $s_k = |\mathbf{f} - \hat{\mathbf{f}}_k|$. $U_k(\cdot)$'s lightweight ($\approx 40M$ parameter) design reduces fine-tuning complexity at the module level.,

3.4 Sampling

Upsampling guidance. Our goal is to leverage the prior information learned during the conditional fine-tuning stage (Sec. 3.2) while ensuring that conditions

are properly propagated through the upsampling process (Sec. 3.3). To achieve this, we combine the conditional generation component $\hat{\mathbf{r}}_k^u$, obtained from the conditional fine-tuning stage, with the conditional component $\hat{\mathbf{r}}_k^c$, produced by the upsampling model $U(\cdot)$ in our conditional upsampling architecture. As seen in fig. 2, these two components are combined at each sampling stage to form the final prediction $\hat{\mathbf{r}}_k$. This integration is achieved using a custom classifier-free guidance approach (Ho and Salimans, 2022) that is defined as:

$$\hat{\mathbf{r}}_k = (1 + w_k)\hat{\mathbf{r}}_k^c - w_k\hat{\mathbf{r}}_k^u, \quad (7)$$

where w_k represents the classifier-free guidance scale applied at scale k , which controls the influence between both components $\hat{\mathbf{r}}_k^u$ and $\hat{\mathbf{r}}_k^c$ on the final output $\hat{\mathbf{r}}_k$.

Scale-wise conditional upsampling. Intermediate predictions $\hat{\mathbf{r}}_k$ across all scales k are required during the hierarchical generation process (see Eq. 2). The straightforward approach to obtaining these intermediate predictions $\hat{\mathbf{r}}_k$ (where $k \neq K$) is to train separate models for each generation scale, with each

Table 2: Ablation on our sampling guidance. We vary only the guidance schedule w_k and report affine-invariant metrics (lower is better for AbsRel; higher is better for δ_1). *No guidance* ($w_k = -1$) disables our sampling contribution; *Constant* uses $w_k = 3.5$ for all scales; *Optimized* is our schedule (guidance off for early scales, on for late scales).

Method	NYU		KITTI	
	AbsRel \downarrow	$\delta_1 \uparrow$	AbsRel \downarrow	$\delta_1 \uparrow$
Ours - optimized w_k	6.4	94.8	10.4	90.1
Ours - $w_k = -1 \forall k$ (no guidance)	12.4	55.7	20.1	70.5
Ours - $w_k = 3.5 \forall k$ (constant guidance)	9.2	85.1	12.1	84.5

model specifically designed to predict upscaled tokens at its corresponding resolution. However, this approach significantly increases computational and training complexity.

Instead, we present the more efficient re-encoding approach. Our conditional upsampling model $U(\cdot)$ is designed to predict the final high-resolution depth encoding $\hat{\mathbf{f}}$ without propagating the intermediate generation scales k . When a prediction at an intermediate scale k is required, we generate the high-resolution prediction using the image-to-image model $U(\hat{\mathbf{f}}_k, \mathbf{c}_k)$, pass it through the VAR encoding scheme, thereby *re-encoding* the high-resolution prediction as a forward pass, and extract the token representation at the desired scale k as:

$$\hat{\mathbf{f}}_k = \mathcal{E}_k(\hat{\mathbf{f}}). \quad (8)$$

Although re-encoding introduces an extra forward pass, this avoids training separate upsamplers for each scale, simplifying the architecture and reducing fine-tuning cost.

4 Experiments

We conduct experiments on five standard scale-invariant depth estimation benchmarks, results can be seen in Tab. 1 and are discussed in the following section. Additionally we present ablations indicating the performance when applying the proposed conditional fine-tuning in combination with the upsampling guidance and ablate on the sampling efficiency.

4.1 Results

Training datasets. Following the existing protocol (Ke et al., 2024; Gui et al., 2025), we employ the Hypersim dataset (Roberts et al., 2021), comprising 461 photorealistic indoor scenes. Images are standardized to 480×640 pixels. In addition we utilize vKITTI (Gaidon et al., 2016), containing 20K additional samples cropped to KITTI benchmark specifications (Geiger et al., 2013). Depth values undergo normalization following (Ke et al., 2024).

Testing datasets. The generalisation capability of the model is evaluated using five different real-world datasets. Each dataset represents a different environmental condition and acquisition process. First, the indoor domain is represented by NYU (Nathan Silberman and Fergus, 2012), comprising 654 RGB-D images from the designated test split, acquired with the Kinect sensor. Additionally ScanNet (Dai et al., 2017), containing 1512 samples is utilized to further investigate the indoor prediction capability of our model. The automotive domain is assessed through KITTI (Geiger et al., 2013), utilizing the Eigen test split configuration with LiDAR-based depth acquisition, representative of outdoor scenes. We additionally employ ETH3D (Schöps et al., 2019), consisting of 454 high-fidelity samples with multi-view stereo reconstruction ground truth, representing additional outdoor scenes. Finally the performance is evaluated on DIODE (Vasiljevic et al., 2019) containing both indoor and outdoor scenes.

Comparison with other methods. Table 1 presents our depth estimation model’s performance against baselines. Our objective is to demonstrate competitive performance under constrained data and compute, without relying on extremely large priors or extensive task-specific fine-tuning. Accordingly, our primary comparison set is limited to methods whose priors are trained on at most 100 million samples and that require fewer than 3 million samples for fine-tuning. These criteria define a practically relevant regime in which neither massive pretraining nor large-scale depth supervision dominates performance.

This setting is particularly relevant for applications such as robotics, embodied perception, and AR/VR, where collecting large annotated depth datasets is costly and rapid adaptation to new domains is preferred over retraining at scale. Within this setting, our approach consistently outperforms nearly all baselines in indoor environments (NYU Eigen split, ScanNet validation split). In outdoor scenarios (KITTI Eigen split, ETH3D), our method delivers competitive performance, though slightly behind the strongest feedforward CNN baselines (DPT (Ranftl

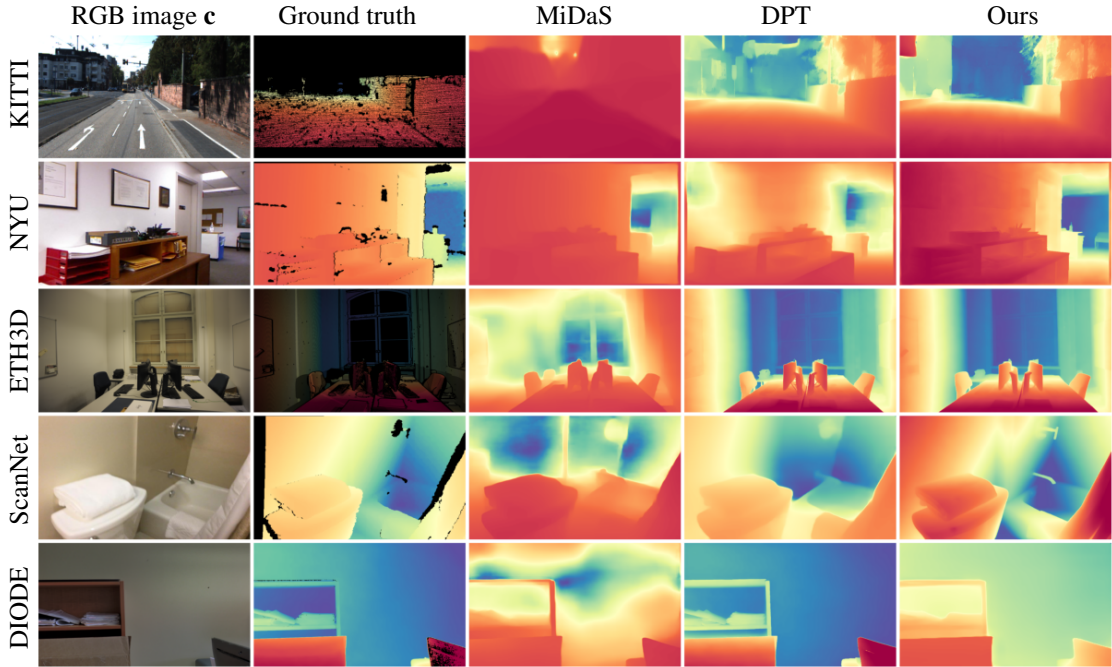


Figure 3: Predictions of Indoor and Outdoor experiments. Additionally we include the Ground truth and the input image provided by the test sets.

et al., 2021), HDN (Zhang et al., 2022)). We attribute this primarily to the domain gap: fine-tuning relies on Hypersim and vKITTI, which emphasize indoor and synthetic driving imagery. Despite this, our model achieves strong outdoor generalization given its modest fine-tuning set and smaller pretraining data. Overall, the performance gap remains narrow, highlighting the effectiveness of visual autoregressive priors in this constrained-data regime.

Implementation details. Our implementation adopts the architectural foundation of VAR (Tian et al., 2024) and the Switti transformer (Voronov et al., 2024). The autoregressive model adapts similar configuration to Switti, yielding a parameter count of approximately 2B. The optimization procedure employs the Adam optimizer (Kingma and Ba, 2014) with a two-phase training protocol. Initial training is conducted on the synthetic vKITTI dataset for 30 epochs, followed by 80 epochs of training on the Hypersim dataset. The optimizer is configured with standard hyperparameters: momentum coefficients $\beta_1 = 0.9$ and $\beta_2 = 0.999$, numerical stability constant $\epsilon = 10^{-8}$, and a learning rate of $\eta = 10^{-6}$. The complete finetuning procedure requires approximately 100 NVIDIA A100 GPU hours.

The conditioning upsampling modules are trained independently using heavily augmented training data,

which includes CutMix augmentations (Yun et al., 2019) and ColorJitter augmentations. For optimization, the Adam optimizer (Kingma and Ba, 2014) is employed with a learning rate of $\eta = 10^{-4}$. The training strategy involves training the model for 10 epochs on vKITTI (Gaidon et al., 2016) and 5 epochs on Hypersim (Roberts et al., 2021). The total training time is approximately 5 hours.

Evaluation protocol. Following the affine-invariant depth estimation paradigm (Ranftl et al., 2020), predictions m are aligned to ground truth d via least-squares fitting: $a = m \times s + t$. Performance is evaluated using two standard metrics (Eigen et al., 2014; Garg et al., 2016; Laina et al., 2016). We employ Absolute Relative Error (AbsRel) and δ_1 accuracy. Computational efficiency is assessed through encoding and decoding latency measurements (in ms) for all evaluated approaches.

Qualitative results. Figure 3 presents depth prediction comparisons across different methods and datasets. As suggested by the quantitative measurements our approach performs very good on NYU and ScanNet, particularly our approach is able to capture the fine structures, such as armrest more reliably. On the KITTI outdoor dataset, our model demonstrates competitive performance with existing approaches. In

Table 3: Inference efficiency comparison. Latency measured on a single A100 GPU. The table emphasizes methods with iterative generative inference. Feedforward CNN baselines (e.g., HDN) are omitted when their inference behavior is representative of other single-pass models. Our VAR approach achieves inference latency comparable to reduced-step diffusion, while being slower and heavier than feedforward CNN baselines. The trade-off is that our method uses substantially fewer pretraining samples than diffusion.

Method	Prior Size	Fine-tune Samples	Inference Steps	Latency (ms)	GPUh
DPT	ImageNet – 14M	1.4M	1	45	> 1000
DepthAnything v2	DINOv2 – 142M	63M	1	55	> 1000 ¹
Metric3D v2	DINOv2 – 142M	16M	1	60	> 1500
Marigold v1.0	SD 2.0 – 2.3B	74K	50×10	4008	~72
Marigold v1.1	SD 2.0 – 2.3B	74K	1×4	172	~72
Marigold E2E	SD 2.0 – 2.3B	74K	1×1	47	~72
Ours (VAR, opt. w_k)	Switti – 100M	74K	10 (scales)	53	~100

particular when compared to MiDaS (Ranftl et al., 2020) our approach is able to indicate richer details, e.g. tree structure. Finally both ETH3D and DIODE demonstrate that our approach is able to detect finer structures such as the window (middle row in Fig. 3), however finer details, such as the window frame are missed.

4.2 Ablation studies

Sampling guidance. We ablate our sampling contribution by varying the classifier-free guidance. $w_k = -1$ disables our proposed guidance (i.e., no conditional combination), reducing the model to a plain VAR prior conditioned only through teacher forcing. A constant schedule with $w_k = 3.5$ applies strong guidance at all scales, while optimized w_k enables guidance only at later scales $k \geq 6$. Table 2 isolates this factor and shows that disabling guidance substantially degrades accuracy across datasets, whereas the optimized schedule yields the best overall results with minimal latency overhead. This confirms that the sampling/guidance mechanism is essential to the final model.

Efficiency. We measure wall-clock inference latency on a single NVIDIA A100 (batch size 1) at the resolution 512×512 in Tab. 3. For feedforward baselines (DPT (Ranftl et al., 2021), DepthAnything (Yang et al., 2024), Metric3D (Hu et al., 2024)), inference consists of a single forward pass. For Marigold, we report both typical multi-step denoising (50 steps) and reduced-step variants (1×1 , 1×4) (Ke et al., 2025; Martin Garcia et al., 2025). Our method requires 10 scale-wise stages, each predicting higher resolution maps, resulting in runtime similar to reduced-step diffusion.

Our method requires 10 scale-wise stages. Each stage predicts an entire resolution map, making runtime comparable to single-step diffusion. While our

approach is somewhat slower than purely feedforward CNN baselines and the model has $\sim 2B$ parameters, it achieves this behavior with orders of magnitude fewer pretraining samples and comparable fine-tuning compute (≈ 100 GPU hours). This highlights a different efficiency–capacity trade-off, where VAR priors provide competitive inference while avoiding pretraining on extremely large datasets.

5 Conclusion

We presented adaptation of visual autoregressive priors for monocular depth estimation. By introducing a scale-wise conditional upsampling mechanism, classifier-free guidance, and a re-encoding strategy, our model achieves state-of-the-art indoor accuracy under constrained training data and competitive outdoor performance. Importantly, it requires 74K synthetic fine-tuning samples and performs inference via 10 fixed scale-wise steps, resulting in sampling speeds comparable to single-step diffusion and slightly slower than feedforward approaches. While the parameter count remains, inference latency is comparable to diffusion-based methods despite using substantially less pretraining. This demonstrates that autoregressive priors achieve performance on par with diffusion while offering a complementary alternative with different trade-offs in training cost and inference structure.

Acknowledgements

Part of the research leading to these results is funded by the German Research Foundation (DFG) within

¹Given the 10^7 – 10^8 image-scale pseudo-labeling/training, the total training compute is plausibly in the thousands to tens of thousands of GPU-hours range; exact figures are not reported.

the project 458972748. The authors would like to thank the foundation for the successful cooperation.

Additionally the authors gratefully acknowledge the scientific support and HPC resources provided by the Erlangen National High Performance Computing Center (NHR@FAU) of the Friedrich-Alexander-Universität Erlangen-Nürnberg (FAU). The hardware is funded by the German Research Foundation (DFG).

REFERENCES

Bhat, S. F., Alhashim, I., and Wonka, P. (2021). Adabins: Depth estimation using adaptive bins. In *Proceedings of the IEEE/CVF Conference on Computer Vision and Pattern Recognition*, pages 4009–4018.

Byeon, M., Park, B., Kim, H., Lee, S., Baek, W., and Kim, S. (2022). Coyo-700m: Image-text pair dataset. <https://github.com/kakaobrain/coyo-dataset>.

Chang, H., Zhang, H., Barber, J., Maschinot, A., Lezama, J., Jiang, L., Yang, M.-H., Murphy, K. P., Freeman, W. T., Rubinstein, M., et al. (2023). Muse: Text-to-image generation via masked generative transformers. In *International Conference on Machine Learning*, pages 4055–4075. PMLR.

Chang, H., Zhang, H., Jiang, L., Liu, C., and Freeman, W. T. (2022). Maskgit: Masked generative image transformer. In *Proceedings of the IEEE/CVF Conference on Computer Vision and Pattern Recognition*, pages 11315–11325.

Dai, A., Chang, A. X., Savva, M., Halber, M., Funkhouser, T., and Nießner, M. (2017). Scannet: Richly-annotated 3d reconstructions of indoor scenes. In *Proceedings of the IEEE conference on computer vision and pattern recognition*, pages 5828–5839.

Eftekhari, A., Sax, A., Malik, J., and Zamir, A. (2021). Omnidata: A scalable pipeline for making multi-task mid-level vision datasets from 3d scans. In *Proceedings of the IEEE/CVF International Conference on Computer Vision*, pages 10786–10796.

Eigen, D., Puhrsch, C., and Fergus, R. (2014). Depth map prediction from a single image using a multi-scale deep network. In Ghahramani, Z., Welling, M., Cortes, C., Lawrence, N., and Weinberger, K., editors, *Advances in Neural Information Processing Systems*, volume 27. Curran Associates, Inc.

El-Ghoussani, A., Hornauer, J., Carneiro, G., and Belagiannis, V. (2025). Consistency regularisation for unsupervised domain adaptation in monocular depth estimation. In *Conference on Lifelong Learning Agents*, pages 577–596. PMLR.

Esser, P., Rombach, R., and Ommer, B. (2021). Taming transformers for high-resolution image synthesis. In *Proceedings of the IEEE/CVF conference on computer vision and pattern recognition*, pages 12873–12883.

Fu, X., Yin, W., Hu, M., Wang, K., Ma, Y., Tan, P., Shen, S., Lin, D., and Long, X. (2025). Geowizard: Unleashing the diffusion priors for 3d geometry estimation from a single image. In *European Conference on Computer Vision*, pages 241–258. Springer.

Gaidon, A., Wang, Q., Cabon, Y., and Vig, E. (2016). Virtual Worlds as Proxy for Multi-Object Tracking Analysis. *arXiv:1605.06457 [cs, stat]*.

Garg, R., Bg, V. K., Carneiro, G., and Reid, I. (2016). Unsupervised cnn for single view depth estimation: Geometry to the rescue. In *Computer Vision–ECCV 2016: 14th European Conference, Amsterdam, The Netherlands, October 11–14, 2016, Proceedings, Part VIII 14*, pages 740–756. Springer.

Geiger, A., Lenz, P., Stiller, C., and Urtasun, R. (2013). Vision meets robotics: the KITTI dataset. *The International Journal of Robotics Research*, 32:1231–1237.

Godard, C., Mac Aodha, O., and Brostow, G. J. (2017). Unsupervised monocular depth estimation with left-right consistency. In *Proceedings of the IEEE conference on computer vision and pattern recognition*, pages 270–279.

Gu, A. and Dao, T. (2023). Mamba: Linear-time sequence modeling with selective state spaces. *arXiv preprint arXiv:2312.00752*.

Gui, M., Schusterbauer, J., Prestel, U., Ma, P., Kotovenko, D., Grebenkova, O., Baumann, S. A., Hu, V. T., and Ommer, B. (2025). Depthfm: Fast generative monocular depth estimation with flow matching. In *Proceedings of the AAAI Conference on Artificial Intelligence*, volume 39, pages 3203–3211.

Han, J., Liu, J., Jiang, Y., Yan, B., Zhang, Y., Yuan, Z., Peng, B., and Liu, X. (2025). Infinity: Scaling bitwise autoregressive modeling for high-resolution image synthesis. In *Proceedings of the Computer Vision and Pattern Recognition Conference*, pages 15733–15744.

Ho, J. and Salimans, T. (2022). Classifier-free diffusion guidance. *arXiv preprint arXiv:2207.12598*.

Hu, M., Yin, W., Zhang, C., Cai, Z., Long, X., Chen, H., Wang, K., Yu, G., Shen, C., and Shen, S. (2024). Metric3d v2: A versatile monocular geometric foundation model for zero-shot metric depth and surface normal estimation. *arXiv preprint arXiv:2404.15506*.

Ke, B., Obukhov, A., Huang, S., Metzger, N., Daudt, R. C., and Schindler, K. (2024). Repurposing diffusion-based image generators for monocular depth estimation. In *Proceedings of the IEEE/CVF Conference on Computer Vision and Pattern Recognition*, pages 9492–9502.

Ke, B., Qu, K., Wang, T., Metzger, N., Huang, S., Li, B., Obukhov, A., and Schindler, K. (2025). Marigold: Affordable adaptation of diffusion-based image generators for image analysis. *arXiv preprint arXiv:2505.09358*.

Kingma, D. P. and Ba, J. (2014). Adam: A method for stochastic optimization. *CoRR*, abs/1412.6980.

Kundu, J., Uppala, P. K., Pahuja, A., and Babu, R. (2018). Adadepth: Unsupervised content congruent adaptation for depth estimation.

Kuznetsova, A., Rom, H., Alldrin, N., Uijlings, J., Krasin, I., Pont-Tuset, J., Kamali, S., Popov, S., Malloci, M., Kolesnikov, A., et al. (2020). The open images dataset v4: Unified image classification, object detection, and visual relationship detection at scale. *International journal of computer vision*, 128(7):1956–1981.

Laina, I., Rupprecht, C., Belagiannis, V., Tombari, F., and Navab, N. (2016). Deeper depth prediction with fully convolutional residual networks. In *2016 Fourth international conference on 3D vision (3DV)*, pages 239–248. IEEE.

Lee, D., Kim, C., Kim, S., Cho, M., and Han, W.-S. (2022). Autoregressive image generation using residual quantization. In *Proceedings of the IEEE/CVF Conference on Computer Vision and Pattern Recognition*, pages 11523–11532.

Li, H., Yang, J., Wang, K., Qiu, X., Chou, Y., Li, X., and Li, G. (2024). Scalable autoregressive image generation with mamba. *arXiv preprint arXiv:2408.12245*.

Liu, C., Kumar, S., Gu, S., Timofte, R., and Van Gool, L. (2023). Va-depthnet: A variational approach to single image depth prediction. In *The Eleventh International Conference on Learning Representations*.

Liu, D., Zhao, S., Zhuo, L., Lin, W., Qiao, Y., Li, H., and Gao, P. (2024). Lumina-mgpt: Illuminate flexible photorealistic text-to-image generation with multimodal generative pretraining. *arXiv preprint arXiv:2408.02657*.

Liu, F., Shen, C., Lin, G., and Reid, I. (2016). Learning Depth from Single Monocular Images Using Deep Convolutional Neural Fields. *IEEE Transactions on Pattern Analysis and Machine Intelligence*, 38(10):2024–2039. arXiv:1502.07411 [cs].

Martin Garcia, G., Abou Zeid, K., Schmidt, C., de Geus, D., Hermans, A., and Leibe, B. (2025). Fine-tuning image-conditional diffusion models is easier than you think. In *Proceedings of the IEEE/CVF Winter Conference on Applications of Computer Vision (WACV)*.

Nathan Silberman, Derek Hoiem, P. K. and Fergus, R. (2012). Indoor segmentation and support inference from rgbd images. In *ECCV*.

Quab, M., Darzet, T., Moutakanni, T., Vo, H., Szafraniec, M., Khalidov, V., Fernandez, P., Haziza, D., Massa, F., El-Nouby, A., et al. (2023). Dinov2: Learning robust visual features without supervision. *Transactions on Machine Learning Research*.

Raffel, C., Shazeer, N., Roberts, A., Lee, K., Narang, S., Matena, M., Zhou, Y., Li, W., and Liu, P. J. (2020). Exploring the limits of transfer learning with a unified text-to-text transformer. *Journal of machine learning research*, 21(140):1–67.

Ranftl, R., Bochkovskiy, A., and Koltun, V. (2021). Vision transformers for dense prediction. In *Proceedings of the IEEE/CVF international conference on computer vision*, pages 12179–12188.

Ranftl, R., Lasinger, K., Hafner, D., Schindler, K., and Koltun, V. (2020). Towards robust monocular depth estimation: Mixing datasets for zero-shot cross-dataset transfer. *IEEE transactions on pattern analysis and machine intelligence*, 44(3):1623–1637.

Razavi, A., Van den Oord, A., and Vinyals, O. (2019). Generating diverse high-fidelity images with vq-vae-2. *Advances in neural information processing systems*, 32.

Richter, T., Seiler, J., Schnurrer, W., and Kaup, A. (2016). Robust super-resolution for mixed-resolution multiview image plus depth data. *IEEE Transactions on Circuits and Systems for Video Technology*, 26(5):814–828.

Roberts, M., Ramapuram, J., Ranjan, A., Kumar, A., Bautista, M. A., Paczan, N., Webb, R., and Susskind, J. M. (2021). Hypersim: A photorealistic synthetic dataset for holistic indoor scene understanding. In *International Conference on Computer Vision (ICCV) 2021*.

Rombach, R., Blattmann, A., Lorenz, D., Esser, P., and Ommer, B. (2022). High-resolution image synthesis with latent diffusion models. In *Proceedings of the IEEE/CVF conference on computer vision and pattern recognition*, pages 10684–10695.

Ronneberger, O., Fischer, P., and Brox, T. (2015). U-Net: Convolutional Networks for Biomedical Image Segmentation. *Lecture Notes in Computer Science*, pages 234–241, Cham. Springer International Publishing.

Rudolph, M., Dawoud, Y., Güldenring, R., Nalpantidis, L., and Belagiannis, V. (2022). Lightweight monocular depth estimation through guided decoding. In *2022 International Conference on Robotics and Automation (ICRA)*, pages 2344–2350. IEEE.

Saxena, S., Herrmann, C., Hur, J., Kar, A., Norouzi, M., Sun, D., and Fleet, D. J. (2024). The surprising effectiveness of diffusion models for optical flow and monocular depth estimation. *Advances in Neural Information Processing Systems*, 36.

Saxena, S., Kar, A., Norouzi, M., and Fleet, D. J. (2023). Monocular depth estimation using diffusion models. *arXiv preprint arXiv:2302.14816*.

Schöps, T., Sattler, T., and Pollefeys, M. (2019). BAD SLAM: Bundle adjusted direct RGB-D SLAM. In *Conference on Computer Vision and Pattern Recognition (CVPR)*.

Schuhmann, C., Beaumont, R., Vencu, R., Gordon, C., Wightman, R., Cherti, M., Coombes, T., Katta, A., Mullis, C., Wortsman, M., et al. (2022). Laion-5b: An open large-scale dataset for training next generation image-text models. *Advances in neural information processing systems*, 35:25278–25294.

Schuhmann, C., Vencu, R., Beaumont, R., Kaczmarczyk, R., Mullis, C., Katta, A., Coombes, T., Jitsev, J., and Komatsuaki, A. (2021). Laion-400m: Open dataset of clip-filtered 400 million image-text pairs. *arXiv preprint arXiv:2111.02114*.

Sun, P., Jiang, Y., Chen, S., Zhang, S., Peng, B., Luo, P., and Yuan, Z. (2024). Autoregressive model beats diffusion: Llama for scalable image generation. *arXiv preprint arXiv:2406.06525*.

Tian, K., Jiang, Y., Yuan, Z., Peng, B., and Wang, L. (2024). Visual autoregressive modeling: Scalable image generation via next-scale prediction. *Advances in neural information processing systems*, 37:84839–84865.

Touvron, H., Lavril, T., Izacard, G., Martinet, X., Lachaux, M.-A., Lacroix, T., Rozière, B., Goyal, N., Hambro, E., Azhar, F., Rodriguez, A., Joulin, A., Grave, E., and Lample, G. (2023). Llama: Open and efficient foundation language models. *ArXiv*, abs/2302.13971.

Van den Oord, A., Kalchbrenner, N., Espeholt, L., Vinyals, O., Graves, A., et al. (2016). Conditional image generation with pixelcnn decoders. *Advances in neural information processing systems*, 29.

Van Den Oord, A., Vinyals, O., et al. (2017). Neural discrete representation learning. *Advances in neural information processing systems*, 30.

Vasiljevic, I., Kolkin, N., Zhang, S., Luo, R., Wang, H., Dai, F. Z., Daniele, A. F., Mostajabi, M., Basart, S., Walter, M. R., et al. (2019). Diode: A dense indoor and outdoor depth dataset. *arXiv preprint arXiv:1908.00463*.

Voronov, A., Kuznedelev, D., Khoroshikh, M., Khrulkov, V., and Baranchuk, D. (2024). Switti: Designing scale-wise transformers for text-to-image synthesis. *arXiv preprint arXiv:2412.01819*.

Wang, Y., Yang, Y., Yang, Z., Zhao, L., Wang, P., and Xu, W. (2018). Occlusion aware unsupervised learning of optical flow. In *Proceedings of the IEEE conference on computer vision and pattern recognition*, pages 4884–4893.

Yang, L., Kang, B., Huang, Z., Zhao, Z., Xu, X., Feng, J., and Zhao, H. (2024). Depth anything v2. *Advances in Neural Information Processing Systems*, 37:21875–21911.

Yin, Z., Shi, J., Li, H., Dai, X., and Lin, X. (2018). Geonet: Unsupervised learning of dense depth, optical flow and camera pose. In *Proceedings of the IEEE Conference on Computer Vision and Pattern Recognition*, pages 1983–1992.

Yu, J., Xu, Y., Koh, J. Y., Luong, T., Baid, G., Wang, Z., Va-sudevan, V., Ku, A., Yang, Y., Ayan, B. K., et al. (2022). Scaling autoregressive models for content-rich text-to-image generation. *Transactions on Machine Learning Research*.

Yu, L., Lezama, J., Gundavarapu, N. B., Versari, L., Sohn, K., Minnen, D., Cheng, Y., Birodkar, V., Gupta, A., Gu, X., et al. (2023). Language model beats diffusion–tokenizer is key to visual generation. *arXiv preprint arXiv:2310.05737*.

Yun, S., Han, D., Oh, S. J., Chun, S., Choe, J., and Yoo, Y. (2019). CutMix: Regularization Strategy to Train Strong Classifiers with Localizable Features. *arXiv:1905.04899 [cs]*.

Zhang, C., Yin, W., Wang, B., Yu, G., Fu, B., and Shen, C. (2022). Hierarchical normalization for robust monocular depth estimation. *Advances in Neural Information Processing Systems*, 35:14128–14139.

Zhang, J., Huang, J., Jin, S., and Lu, S. (2024). Vision-language models for vision tasks: A survey. *IEEE Transactions on Pattern Analysis and Machine Intelligence*.

Zhou, T., Brown, M., Snavely, N., and Lowe, D. G. (2017). Unsupervised learning of depth and ego-motion from video. In *Proceedings of the IEEE Conference on Computer Vision and Pattern Recognition*, pages 6619–6627.